Alternative Auto-Encoder for State Estimation in Distribution Systems With Unobservability

Priyabrata Sundaray, *Graduate Student Member, IEEE*, and Yang Weng, *Senior Member, IEEE*

***Abstract*—The landscape of energy systems is ever changing due to the introduction of distributed energy resources (DERs) on the generation side and new demand-response technologies on the demand side. This ever-changing landscape calls for accurate real-time monitoring of distribution networks. However, the low observability in the secondary distribution grids makes monitoring hard, due to limited investment in the past and the vast coverage of distribution grids. To recover measurements for robustness, past methods proposed machine learning models by approximating mapping rules. However, mapping rule learning using traditional machine learning tools is one way only, from measurement variables to the state vector variables. Usually, it is hard to be reverted, thereby losing information consistency. This loses the physical relationship on invertibility for applications, such as state estimation. Hence, we propose a structural deep neural network to provide a robust two-way functional approximation. The proposed alternative auto-encoder includes constraints in the latent layer according to available voltage measurements for ensuring two-way information flow and utilizes symbolic regression using the latent variables for explainability. For using physics to regulate the mapping rule, we embed non-linear power flow kernels into the decoder of a variational auto-encoder to regulate both forward and inverse mapping simultaneously. The proposed method of system physics recovery is validated extensively using the IEEE standard distribution test systems. Simulation results show highly accurate two-way information flow.**

***Index Terms*—Distribution system state estimation (DSSE), alternative auto-encoder, two-way information flow, symbolic regression.**

I. Introduction

DISTRIBUTED energy resources (DERs) in the United States have grown almost three times faster than the net total generation capacity from 2015 to 2019 [1]. The global annual investments in DERs are projected to increase by 75% by 2030 as well [2]. With this growth, the penetration of renewables and DERs is projected to increase almost two-fold by 2030 and by more than three-fold by 2050 [3]. With more active devices in the distribution grid, new dynamics are introduced into the grid. Due to this, traditional passive control methods need to be adapted into active control methods to maintain the sustainability of the distribution grids [4], [5] and prevent outages [6].

For controlling power systems, state estimation is the key [7]. But, the prerequisite for state estimation is the need for complete system information, which does not hold for distribution grids in general, especially in secondary distribution grids. It is primarily due to two major factors. First, the limited instrumentation at the edge of the grid [8], [9] results in a scarcity of measurements [10], [11]. It poses a challenge to estimating the voltage phasors of all buses, which represent the distribution system state estimation (DSSE) task [12]. Hence, to know the accurate state of the system, real-time measurements have to be augmented with a high number of pseudo-measurements when performing DSSE [9], [13]. However, pseudo-measurements are much less accurate than real-time measurements and adversely affect the accuracy of the state estimates [14]. Second, in addition to the issue of limited measurements, network topology and line parameters are typically assumed to be perfectly known in the DSSE framework [14], [15]. But, such a fact does not hold for secondary distribution grids due to aging network infrastructure and lack of system monitoring [16], [17]. Considering these challenges, innovative and robust state estimation methods are crucial, especially for secondary distribution networks for sustainable system operation [18].

One way to do state estimation is to use discriminative learning to learn the regression rule from the set of measurement variables to the set of state vector variables. To this end, a number of works have explored using the measurement data itself. These methods use machine learning as a tool. For example, probabilistic and data-driven methods utilize the detection and identification of physical topology [19], [20], [21], [22], [23], [24], [25]. In addition to using topological information, one can embed physics in the mapping rule learning with various machine learning tools [15], [26], [27], [28], [29], [30]. Although these methods show some physical understanding of learning, they can not handle inconsistency in the two-way mapping rule learning for physical systems. This is due to the challenge with data-driven learning algorithms in which typically the mapping is one way only, from measurement variables to the state vector variables, and can not be reverted. To resolve this issue, auto-encoders are introduced into the state estimation for distribution systems. These models map measurement variables to state vectors, which have

Manuscript received 14 January 2022; revised 18 May 2022 and 19 August 2022; accepted 29 August 2022. Date of publication 7 September 2022; date of current version 21 April 2023. This work was supported in part by the Department of Energy under Grant DE-AR00001858-1631 and Grant DE-EE0009355; and in part by the National Science Foundation (NSF) under Grant ECCS-1810537, Grant ECCS-2048288, and Grant AFOSR FA9550-22-1-0294. Paper no. TSG-00062-2022. *(Corresponding author: Yang Weng.)*

The authors are with the School of Electrical, Computer and Energy Engineering, Arizona State University, Tempe, AZ 85281 USA (e-mail: sundaray@asu.edu; yang.weng@asu.edu).

Color versions of one or more figures in this article are available at https://doi.org/10.1109/TSG.2022.3204524.

Digital Object Identifier 10.1109/TSG.2022.3204524

the capability to reconstruct measurement variables to create a two-way mapping.

When the system is observable in a well-monitored area, there are past works utilizing auto-encoder. For example, [31], [32] assume full system knowledge and uses an auto-encoder to reconstruct missing data in state estimation with auto-encoders for smart grid. In addition, to reconstruct missing information for new inputs, an auto-encoder based approach for noisy dataset in [33], [34] focuses on transmission grids, and a probabilistic deep auto-encoder based approach in [35], reconstructs power system measurements to capture the uncertainty information of the measurement data. But these methods still assume good system knowledge. Therefore, it remains open on how to design auto-encoder for systems with unobservability, with confidence. In addition, many physics-informed learning methods are time-consuming due to excessive parameter tuning process and a lot of data for training. To resolve this issue, [36] proposes a composite regularization-based network selection approach to select features to reduce the time of the parameter tuning process. But, these methods still do not take into account the system physics consideration, which can help with narrowing down the learning space further.

Considering the advantages of the two-way information flow, we implement the same by designing a structural deep neural network container to perform forward and inverse mappings in a partially observable system. As the system is only partially observable, we embed knowledge of the network size into the latent layer. The structural neural network utilizes a data-driven method to learn the mapping functions of the system, and the symbolic regression learns the system parameters. The main contributions of the proposed method are four-fold. [i] The first innovation we provide is a two-way mapping function using a structural deep learning container to introduce physical knowledge to regularize the learning of forward and inverse mapping consistency for future operating points in a partially observable system. [ii] Second, the latent unit is created to embed knowledge of the network size into the latent layer. [iii] Third, we improve the computational complexity by utilizing the spatial data of location and topology corresponding to the observable nodes obtained from the GIS information database. [iv] Finally, to provide confidence for system operators on the edge using our design, we show how to bound the uncertainty systematically.

Based on the contributions of the proposed model discussed above, these are validated numerically in a diverse selection of power grid transmission and distribution test cases from MATPOWER [37]. The test cases include 4-bus, 5-bus, 9-bus, 14-bus, 18-bus, 22-bus, 33-bus, 69-bus, 85-bus, 123-bus, 141-bus and 8500-bus IEEE test cases. Using numerical tests on this wide selection of power system cases, the proposed method is validated for its effectiveness and robustness. Hence, the introduction of constraints improves the learning capability for the mapping to very high accuracy.

The remainder of this paper is organized as follows. The problem modeling is described in Section II. The specifics of the proposed method are presented in Section III. To understand the forward-mapping component of the network, it is explained in Section III-A. To infer the partial knowledge in presence of unobservability, the setup is described in Section III-B, and the inverse mapping is discussed in Section III-C. The integration of the forward, intermediate, and inverse mappings along with the combination of the symbolic regression is presented in Section III-D. Section IV presents the proof of the uncertainty quantification to bound the uncertainty of the model. The numerical validation is presented in Section V. Finally, we draw the conclusion in Section VI.

II. Problem Modelling

In a power distribution system, when a node is partially observable, the voltage magnitude and voltage phase angle values are unknown. This partial observability in the topology impacts the calculation of active and reactive power injections at the neighboring buses. Although the power injection is coupled to the voltage components algebraically, it becomes difficult to use the power flow method to realize the algebraic relationship in the presence of partial observability. Therefore, in the absence of any algebraic relationship, a data-driven method needs to be employed to obtain the relationship between the power injection and the voltage components to estimate the system parameters. In obtaining the system parameters, knowledge of the physical system that governs the relationship between the power and voltage measurements is used. This, in turn, can be utilized to determine power injection by the neighboring buses to the unobservable nodes, which otherwise would not have been possible to obtain by solving power flow equations. In model-X, the voltage and power components may not necessarily be from the same observable bus. The way we deal with it has been discussed in Section III-B.

The DSSE relies on a general model [13], which can be represented as: $y = f(x) + \epsilon$, where y represents the vector of the measurements obtained from the network as well as from the pseudo-measurements. x represents the state vector, f in general represents the vector of non-linear measurement functions, and ϵ represents the measurement noise vector, which is usually assumed to be composed of independent zero-mean Gaussian variables. In practical cases, most state estimation programs are formulated as over-determined systems of nonlinear equations. These types of systems are solved as weighted least squares (WLS) problems [38]. In the WLS approach, the estimation of state x is usually obtained by the minimization of the weighted sum of the squares of the residuals. The residual is defined as the difference between the measurement variable, y_i and the value obtained by using the model, $f(x_i)$, which is described as follows:

$$\arg\min_{x} \sum_{i=1}^{k} w_i (y_i - f_i(x))^2, \tag{1}$$

where w_i denotes the weight associated with the i^{th} measurement, and k is the total number of available measurements. In a distribution system, complete system information is usually not available for monitoring and control purposes, especially in the secondary distribution grids. So, when a node is partially observable, the state vectors corresponding to the unobservable subsystem are unknown. This partial observability in the topology impacts the calculation of measurement variables at the neighboring buses. In a distribution grid with underlying physics governing the system, the measurement variables are coupled with the state vectors algebraically. However, in presence of partial observability, it becomes difficult to realize the algebraic relationship. Therefore, as discussed in Section I, with partial observability in a system, a data-driven method needs to be employed to obtain the relationship between the measurement variables and state vectors to estimate the system parameters. However, approximation of the system parameters using traditional machine learning methods has three disadvantages. First, it does not consider the relationship between variables, thereby ignoring the system physics. Second, it results in inconsistent mapping through one-way information flow. Thereby losing the information by one-way information flow, as the measurement variables in the system are not reproducible. Lastly, it is combinatorial in nature and is thereby computationally complex. Hence, we have designed an algorithm that uses a two-way information flow for a consistent mapping to solve the system equation without an accurate system model.

In addition, system parameters are utilized to determine sensor measurements corresponding to neighboring buses to the unobservable nodes, which otherwise was not possible by solving parametric system equations. Thus, Model-X has the capability to estimate parameters associated with the unobservable nodes, which otherwise was not possible. The reason to estimate all the system parameters is that the work is focused on secondary distribution grid. The parameters in the case of secondary distribution grid are usually unknown. So, these parameters are not present in the database. Even if the parameters are available in the database, those values cannot be trusted. This argument is applicable even to primary distribution grids, where the parameters are known only at certain locations.

Since only physical laws can create a two-way mapping with consistent results, so we design a structural deep neural network container to perform forward and inverse mappings in a partially observable system. Although the system is only partially observable, we embed knowledge of the system size into the latent layer. There are two benefits of such a design. One is that we can ensure that the learner keeps enough information to recover the encoder input at the output side of the decoder. This is a critical design in our physics-auto-encoder, as our primary rule is not to compress information in the latent layer but to maintain just the right information in the latent state layer. Another benefit of embedding system size into the latent layer is to make the latent layer with a physical meaning of the system state. So, these state measurements will guide the rest of the latent variables to recreate latent units that can uniquely recreate all the measurements for the distribution system uniquely. This has been discussed in detail in Section III-B of the paper.

The specific benefits the two-way information flow provides, are two-fold. First, two-way mapping considers physical knowledge to regularize the learning of mapping rules for future operating points. This is possible due to the learning that is physically meaningful. Thus, the mapping rule hence learned can work in the future with arbitrary operating points. And, second, the two-way mapping rule considers system physics to create the forward and inverse mappings with consistent results. Thus, it is possible to achieve superior mapping capability to learn the underlying physical information of the systems, even with limited observability. This leads to design consistency and trust in machine learning tools on the edge of the grids.

NOTATION

The bold letters are used to denote vectors and vector functions; lower case letters denote scalars and scalar functions. Subscripts are used to indicate a subset. The term $\hat{x}$ indicates the expected value of x. The use of curly braces represents a set of variables. Furthermore, we denote $\boldsymbol{p} = \{p_1, \ldots, p_n\}^T$, $\boldsymbol{q} = \{q_1, \ldots, q_n\}^T$, $\boldsymbol{y} = \{\boldsymbol{p}^T, \boldsymbol{q}^T\}^T$, and $\boldsymbol{v} = \{v_1, \ldots, v_n\}^T$, $\boldsymbol{\phi} = \{\phi_1, \ldots, \phi_n\}^T$, $\boldsymbol{x} = \{\boldsymbol{v}^T, \boldsymbol{\phi}^T\}^T$, with n being the number of buses in the power system case under consideration. In addition to the description of the problem structure, $\mathcal{O}$ and $\bar{\mathbb{O}}$ represent the notations for the set of components in the observable and unobservable subsystems, respectively. In the observable subsystem the corresponding set of variables are represented as $\{(x^i_{\mathcal{O}}, y^i_{\mathcal{O}})\}^k_{i=1}$, with k being the number of samples in the observable subsystem. Similarly, in the unobservable subsystem, the estimate of the corresponding set of variables is represented as $\{(x^i_{\bar{\mathbb{O}}}, y^i_{\bar{\mathbb{O}}})\}^{k'}_{i=1}$, with k' being the number of samples in the unobservable subsystem.

III. PROPOSED METHOD - MODEL-X FOR SYSTEM MONITORING IN PARTIAL OBSERVABILITY

For the proposed method, to solve forward and inverse mapping consistency, the first innovation we provide is a two-way mapping function using a structural deep learning container. First, the mapping from measurement variables $\boldsymbol{y}$ to state vectors $\boldsymbol{x}$ is referred to as a forward mapping. So, forward mapping is defined as a projection from measurement variables to the state vectors via a structural deep neural network. Second, the mapping from state vectors $\boldsymbol{x}$ to measurement variables $\boldsymbol{y}$ is referred to as inverse mapping. Using this, the measurement variables of the system are reproducible. Thus, inverse mapping involves the mapping from the state vectors to the measurement variables, thereby reconstructing the measurement variables. Therefore the name is two-way, one way for mapping measurement variables to the state variables, and the other way for reconstructing the measurement variables.

Therefore, the proposed approach learns the underlying system physics using a machine learning model with physical meaning, and the hidden state simultaneously. Further, to ensure consistent mapping rules, we implement the forward and inverse mappings together when optimizing the machine learning model. This is an extension of the traditional state estimation process, which targets mapping for voltages only. However, to deal with the uncertainty arising out of the unobservability in the system, intermediate mapping is used. The mapping from state vectors $\boldsymbol{x}$ to latent units is referred to as an

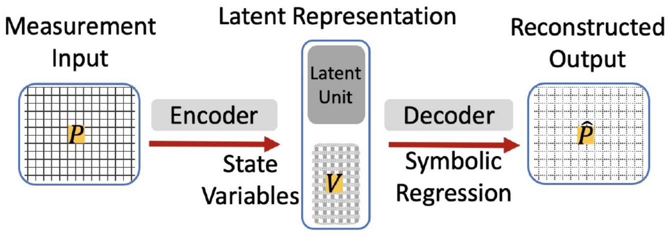

Fig. 1. General architecture of the auto-encoder for model-X.

intermediate mapping. Hence, the sensor information is used to map from the state vectors $\boldsymbol{x}_{\mathcal{O}}$ to learn the latent units $\boldsymbol{x}_{\bar{\mathbb{O}}}$. This involves embedding the network size into the latent layers, which is discussed in detail in Section III-B.

However, neither the forward nor the intermediate mapping, estimate any system parameters explicitly. So, the next innovation we provide is performing the inverse mapping using symbolic regression to estimate the system parameters. Hence, inverse mapping from the latent variables $\boldsymbol{x}_{\mathcal{O}}, \boldsymbol{x}_{\bar{\mathbb{O}}}$ to the measurement variables $\boldsymbol{y}$ yields the estimation for system parameters by using symbolic regression. Therefore, the measurements are reconstructed by using the state vectors and the latent units in the latent layer. As $\boldsymbol{x}_{\bar{\mathbb{O}}}$ is unobservable throughout the mapping, the estimate of $\boldsymbol{x}_{\bar{\mathbb{O}}}$ obtained from the intermediate mapping is considered for the inverse mapping for estimation of system parameters. As the data mining technique used here does not require any system parameters, the need for an accurate system model is eliminated as a result.

The general framework of the auto-encoder architecture for model-X is shown in Figure 1. In our design, the input to the encoder and the output of the decoder are the same, which are the measurement variables. In the literature, different state variables such as voltages, currents, and powers have been considered for the modeling problem in different forms of polar or rectangular coordinates, depending on the need and the availability. In the case of model-X, the active and reactive power components are considered as measurement values at the encoder input and decoder output owing to their availability and relevance in the physical systems. Further, the voltage magnitude and phasor values are considered as the state vectors at the latent layer of model-X. In addition, although the system is only partially observable, we embed knowledge of the network size into the latent layer. So, the state vectors help in the generation of the latent units to estimate the uncertainty in the system arising out of the unobservability. As a result, the state measurements will guide the rest of the latent variables to extract a state set called latent units that can uniquely recreate all the measurements in the distribution system uniquely.

It is important to note here that in the case of model-X, measurements associated with observable nodes are utilized for the estimation, while those associated with unobservable nodes introduce noise. Therefore, the noise for model-X comes from the unobservability alone. In addition, model-X involves the mapping of information corresponding to observable nodes and it has the capability to estimate the system parameters associated with the unobservable nodes. Hence, independent of whether the observable parameters are reliably stored in the database, model-X will be able to perform well, by either utilizing the advantage of the mapping function or by using the reliable parameters corresponding to the observable nodes.

A. Forward Mapping: Physics Informed Analytic Network

To estimate the model of a system utilizing a data-driven method, the mapping functions of the system need to be learned. To learn the mapping functions, an analytical model will be used, which would enhance the understanding of the system. To this end, a network structure is set up to understand the system mathematically. Let us consider a generalized equation to represent the structure of the system model. Hence, to understand the network structure, a generalized mapping function is utilized to map the power measurements $\boldsymbol{y}$ to the voltage measurements $\boldsymbol{x}$ of the system, which is represented by the Equation $\boldsymbol{x} = f_{\boldsymbol{\theta}}(\boldsymbol{y}) + \epsilon$. For the mapping, the network information for the analytic network is represented by $f_{\boldsymbol{\theta}}$, where the function $f_{\boldsymbol{\theta}}$ represents the underlying physics of the system, and ϵ represents the additive noise.

As we define forward mapping as a projection from measurement variables to the state vectors via a structural deep neural network. Therefore, the encoder is mapping the measurement variables to the state vectors in the latent layer. Mathematically, the set of $\{\boldsymbol{y}_{\mathcal{O}}, \boldsymbol{x}_{\mathcal{O}}\}$ variables are coupled algebraically. Considering this coupling, the forward mapping between these variables can be inferred upon exploring the observable subsystem. The forward mapping from measurement variables to the state vectors involves the optimization, as shown in Equation (2).

$$\arg\min_{\boldsymbol{\theta}_1} \left\| f_{\boldsymbol{\theta}_1}(\boldsymbol{y}_{\mathcal{O}}) - \boldsymbol{x}_{\mathcal{O}} \right\|_2^2 \tag{2}$$

where $\boldsymbol{\theta}_1$ denotes the set of learned parameters of $f_{\boldsymbol{\theta}_1}$. The target function denoted by $f^*_{\boldsymbol{\theta}_1} : \boldsymbol{y}_{\mathcal{O}} \rightarrow \boldsymbol{x}_{\mathcal{O}}$ satisfying $\boldsymbol{x}_{\mathcal{O}} = f^*_{\boldsymbol{\theta}_1}(\boldsymbol{y}_{\mathcal{O}})$ learns the forward mapping function.

B. Intermediate Mappings: Preserving Complete Information on Physical States

The forward mapping can be inferred from the algebraic coupling between observable measurements. However, in the presence of partial observability, one needs additional information to infer knowledge about the partial state of the system. Therefore, in model-X, knowledge about the latent layer is vital to understanding the physics of the distribution system. Different than the normal auto-encoder, we constrain the latent layer and create an intermediate mapping in the model-X. The intermediate mapping will map from limited but observable state vectors to the latent units in the latent layer. Therefore, we utilize limited sensors in the latent layer to guide other latent variables to create state sets called latent units, keeping the capability of full physical reconstruction and unit consistency. We constrain the total number of system states including both the state vectors and latent units to be equal to the physical network size. This means that we can determine the number of latent units needed to make the model more physical. Therefore, the intermediate mapping function in the model-X is defined as the mapping using which the latent unit is created to embed knowledge of the network size

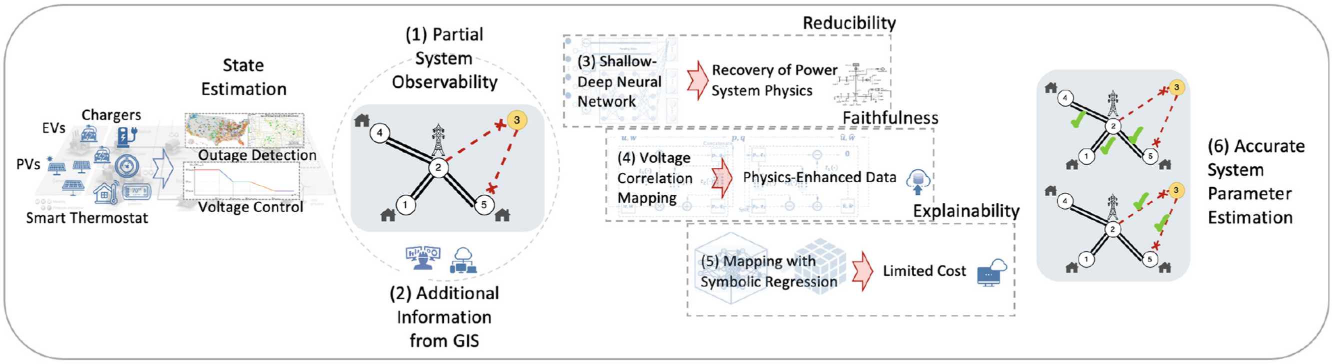

Fig. 2. Framework of constrained neural network model.

into the latent layer. The benefit of such a design is that we can ensure that the learner keeps enough information to recover the encoder input at the output side of the decoder. This is a critical design in our physics-auto-encoder.

Such a constraint design is critical to the performance of model-X, because of the following reasons. If we place less than the sufficient latent units, there is a data compression property like the auto-encoder. However, our objective is not to compress the information, but to compactly represent all possible variables of the energy system in the model-X. If we place more than the adequate number of latent units, then it will distort the physical meaning, e.g., create features that distort the physical meaning of the latent units. Additionally, constraining the number of latent variable to be the same as the network size makes the system states useful. This is because some of the state vectors are observable, which guide the latent units within the latent layer and estimate them. The mathematical formulation is as shown in Equation (3).

$$\arg\min_{\boldsymbol{\theta}_2} \left\| \boldsymbol{x}_{\bar{\mathbb{O}}} - f_{\boldsymbol{\theta}_2}(\boldsymbol{x}_{\mathcal{O}}) \right\|_2^2, \tag{3}$$

where $\boldsymbol{\theta}_2$ denotes the set of learned parameters of $f_{\boldsymbol{\theta}_2}$. The target function denoted by $f^*_{\boldsymbol{\theta}_2} : \boldsymbol{x}_{\mathcal{O}} \rightarrow \boldsymbol{x}_{\bar{\mathbb{O}}}$ satisfies $\boldsymbol{x}_{\bar{\mathbb{O}}} = f^*_{\boldsymbol{\theta}_2}(\boldsymbol{x}_{\mathcal{O}})$ and learns the intermediate mapping function for obtaining state vector correlation.

The model-X is robust to the distribution of load profile and variability in line impedance and requires a rational assumption of correlation of load demand in the power distribution grid. This is to ensure an accurate intermediate mapping because as the load demands are correlated, the voltage phasors obtained are also correlated. The assumption of the correlation can be attributed to the behavior of individual nodes, which exhibits a mutual correlation because of many coupling factors, as mentioned in [39]. These factors include outside temperature, the destination of use, time of the day, etc. To understand the mappings and the logical flow of the proposed data-driven model, the basic framework for the model-X is shown in Figure 2.

C. Inverse Mappings: Embedding All Physical Possibilities

By using forward and intermediate mapping, the mapping function and the latent units are obtained. However, to estimate the system parameters, inverse mapping of the state vectors to the measurement variables is required. Hence, the inverse mapping objective function involves the optimization as shown in Equation (4).

$$\arg\min_{\boldsymbol{\theta}_3} \left\| \boldsymbol{y}_{\mathcal{O}} - f_{\boldsymbol{\theta}_3}\left(\boldsymbol{x}_{\mathcal{O}}, \boldsymbol{x}_{\bar{\mathbb{O}}}\right) \right\|_2^2, \tag{4}$$

where $\boldsymbol{\theta}_3$ denotes the set of learned parameters of $f_{\boldsymbol{\theta}_3}$. The target function denoted by $f^*_{\boldsymbol{\theta}_3} : \{\boldsymbol{x}_{\mathcal{O}}, \boldsymbol{x}_{\bar{\mathbb{O}}}\} \rightarrow \boldsymbol{y}_{\mathcal{O}}$ satisfies $\boldsymbol{y}_{\mathcal{O}} = f^*_{\boldsymbol{\theta}_3}(\boldsymbol{x}_{\mathcal{O}}, \boldsymbol{x}_{\bar{\mathbb{O}}})$ and learns the inverse mapping function. The term $\boldsymbol{x}_{\bar{\mathbb{O}}}$ indicates the estimated value of the latent unit. To understand the mappings and the logical flow of the proposed data-driven model, the basic architecture for the model-X is shown in Figure 2.

However, the explainability of model-X is due to the symbolic regression portion of the proposed method. So, the symbolic regression is performed with the optimization to recover the inverse mapping function. For the inverse mapping, we employ symbolic regression using all possible basis functions (Θ). The symbolic library function consists of all possible polynomial terms resulting from a combination of voltage components. The voltage components are the result of combined voltage terms corresponding to the observable nodes as well as the latent units hence obtained by using the intermediate mapping. However, power systems provide us with a piece of unique knowledge about the special quadratic relationship between the voltage and power components, which are known before modeling. Therefore, using this knowledge about the power systems inverse mapping is performed. The inverse mapping includes an ℓ_1 regularized regression which is performed to select the components responsible for or contributing to the inverse mapping. Due to the ℓ_1 regularized regression, useful feature selection happens in terms of voltage component terms contributing to the power component estimation. This represents the system parameters associated with the observable as well as the unobservable subsystem of the power grid.

The symbolic library function (Θ) is formed by using a combination of terms from $\boldsymbol{x}_{\mathcal{O}}$, and $\boldsymbol{x}_{\bar{\mathbb{O}}}$ based on the prior knowledge about the system, which includes the physical laws governing the system. Therefore, the basis functions are selected based on that prior knowledge, which represents the underlying physical model of the system. This selection is made by performing an ℓ_1 regularized regression. Thus, the

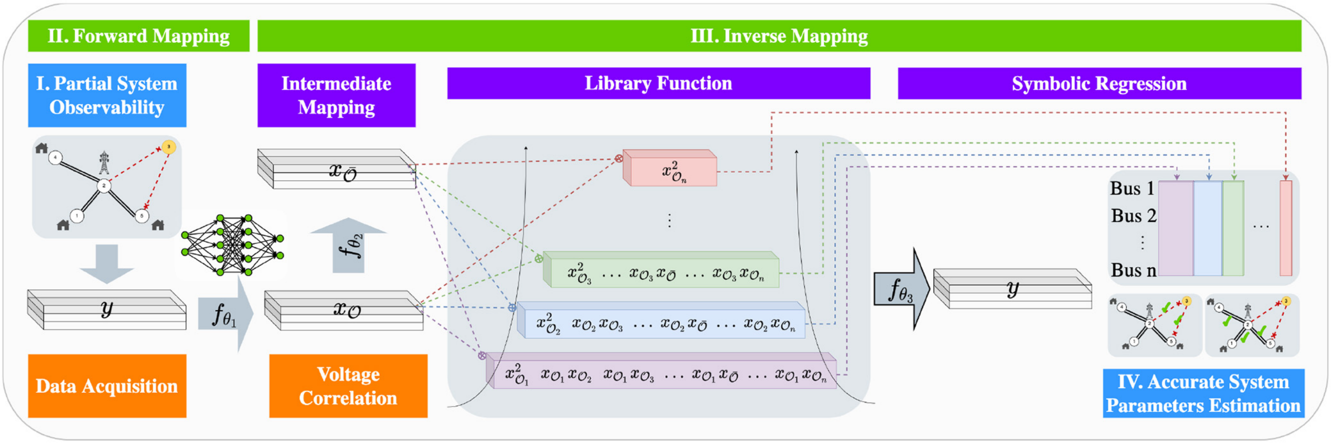

Fig. 3. Architecture of the proposed Model-X, a physics constrained neural network integrated with a symbolic regression.

Equation (4) is transformed to Equation (5).

$$\arg\min_{\boldsymbol{w}} \left\| \boldsymbol{y}_{\mathcal{O}} - \boldsymbol{w}^T \Theta \right\|_2^2 + \beta \|\boldsymbol{w}\|_1, \tag{5}$$

where β is the hyper-parameter for ℓ_1 regularization with $\boldsymbol{w}$ representing weights of the variables corresponding to the symbolic function terms. The reason for using ℓ_1 regularization for inverse mapping in this work as opposed to ℓ_2 regularization is that the ℓ_1 norm performs better than a ℓ_2 norm in terms of useful feature selection. In model-X, the functional mapping f_{θ_3} is obtained by optimizing the inverse mapping using symbolic regression. Therefore, using symbolic regression improves the explainability of model-X in terms of the library function, which contributes to the estimation of the physical laws corresponding to non-zero coefficient values only. Whereas those coefficients corresponding to all the other terms become zero, thereby indicating the set of coupling terms responsible for the physical relationship between the measurement variables and state vectors. Hence, the explainability is achieved in terms of those voltage terms which contribute towards the power components estimation, whose byproduct is the power systems parameters.

D. Combined Objective for the Proposed Model X

The architecture of the detailed model is visualized in Figure 3. The complete objective function for the model-X proposed in this work, using a symbolic regression for the inverse mapping, is described in Equation (6). This equation is obtained by combining Equations (2), (4), and (5). This equation represents the objective function to be optimized for estimating the system parameters.

$$\begin{aligned} arg\min_{\psi} \; \Big\{ & \left\| \boldsymbol{x}_{\mathcal{O}} - f_{\theta_1}(\boldsymbol{y}_{\mathcal{O}}) \right\|_2^2 + \left\| \boldsymbol{x}_{\bar{\mathbb{O}}} - f_{\theta_2}(\boldsymbol{x}_{\mathcal{O}}) \right\|_2^2 \\ & + \left\| \boldsymbol{y}_{\mathcal{O}} - \boldsymbol{w}^T \Theta \right\|_2^2 + \beta \|\boldsymbol{w}\|_1 \Big\}, \end{aligned} \tag{6}$$

where $\psi = \{\boldsymbol{\theta}_1 \cup \boldsymbol{\theta}_2 \cup \boldsymbol{w}\}$ denotes the set of learned parameters of the model with Θ denoting the symbolic library terms obtained from the set of $\{\boldsymbol{x}_{\mathcal{O}}, \boldsymbol{x}_{\bar{\mathbb{O}}}\}$. In Equation (6), the first term performs the forward mapping operation, and the second term performs the intermediate mapping operation for estimating $\boldsymbol{x}_{\bar{\mathbb{O}}}$. The third term in Equation (6) performs the estimation of system parameters. Therefore, by introducing a latent variable, we are able to estimate the state of the observable subsystem and extract useful features from the unobservable subsystem simultaneously.

This is a fundamental change to the problem of system model approximation. With this system model approximation, system parameters are estimated from measurement variables alone. In Equation (6), $\boldsymbol{x}_{\mathcal{O}}$, and $\boldsymbol{y}_{\mathcal{O}}$ are the known terms, while Θ depends on the estimates $\boldsymbol{x}_{\bar{\mathbb{O}}}$. The mapping functions $f_{\boldsymbol{\theta}_1}$, $f_{\boldsymbol{\theta}_2}$, and the model parameter $\boldsymbol{w}$ are the target variables of the optimization function. The objective of the optimization function is to obtain the term $\boldsymbol{w}$, which contains the system parameters. Thus, by combining a symbolically informed latent layer with the proposed constrained neural network, an improvement in the model approximation is achieved, which is presented in Section V-C. This improvement is applicable to components corresponding to both the observable and unobservable subsystems.

The algorithm for the proposed method is summarized in Algorithm 1.

E. Algorithm Overview

The Algorithm 1 considers the values for nodal voltage and power measurements corresponding to the observable nodes as input. It is important to note that the parameters corresponding to the observable nodes can be computed by using linear regression. However, to estimate the parameters corresponding to the unobservable nodes, we need model-X.

F. Requirements for Amount of Data Points

For each of the IEEE standard power system models, the number of data points required for accurate estimation of the system parameters is determined. This determination is performed based on a hyper-parameter which is the size of the inverse mapping parameter space. Based on that hyper-parameter, the required instances of data points are generated. Each generated instance represents a randomly generated set of values for the power and voltage measurements corresponding to all the buses. Considering these measurement values, the

Algorithm 1: Training Algorithm for Physics Constrained Symbolic Network via ℓ_1 - Norm

Data: $G = \{\boldsymbol{y}_{\mathcal{O}}, \boldsymbol{x}_{\mathcal{O}}\}$ such that G is the set of power and voltage measurement variables in the observable subsystem.

Result: Forward and Inverse mapping yielding System parameters

begin

Check: $G \neq \emptyset$

while *Error converges* **do**

1. Map $\boldsymbol{y}_{\mathcal{O}}$ to $\boldsymbol{x}_{\mathcal{O}}$ using a deep neural network.

2.*a*. Estimate $\boldsymbol{x}_{\bar{\mathbb{O}}}$ from $\boldsymbol{x}_{\mathcal{O}}$ using physically informed latent constraint: $arg\min_{\boldsymbol{\theta}_2} \|\boldsymbol{x}_{\bar{\mathbb{O}}} - f_{\boldsymbol{\theta}_2}(\boldsymbol{x}_{\mathcal{O}})\|_2^2$;

2.*b*. Create symbolic library function using $\boldsymbol{x}_{\mathcal{O}}$ and $\boldsymbol{x}_{\bar{\mathbb{O}}}$: (Θ).

3. Combine the physically informed latent constraint with a symbolic regression: $arg\min_{\boldsymbol{w}}\{\|\boldsymbol{y}_{\mathcal{O}} - \boldsymbol{w}^T\Theta\|_2^2 + \beta\ \|\boldsymbol{w}\|_1\}$.

4. Using GIS information, obtain the observable system parameters $w_{\mathcal{O}}$: $arg\min_{w_{\mathcal{O}}}\{\|\boldsymbol{y}_{\mathcal{O}} - w_{\mathcal{O}}^T\boldsymbol{x}_{\mathcal{O}}\|_2^2\}$.

5. Perform multi-objective optimization upon combining the objectives from Step-1, and Step-3, and by considering the constraints from Step-4, to estimate the complete system parameters $(\boldsymbol{w})$.

end

end

active and reactive power injections at each of the nodes are calculated using Equation (9). Followed by this, a power flow study is performed for each measurement data case to obtain the steady-state voltage magnitude and voltage phase angle at all the buses for that particular measurement data. This is detailed in Section V-B. Since one of the buses is assumed as an unobservable component, it cannot be observed for analysis purposes. It is important to note that the power flow calculations are performed by maintaining the ground truth for all the nodes, including the unobservable nodes. It impacts the real and reactive power injection calculations. However, analyses are performed by considering the unobservable nodes as unknown. As a result, the unobservable nodes are considered as optimization parameters. The theoretical guarantee providing invertibility of library function matrix and the matrix sizes for the different model-X components are presented below.

1) Ensuring Invertibility Theoretical Guarantee: Considering there are n_{NOI} number of nodes directly interacting with the unobservability, there are n_{NOI} sets of susceptance and conductance values associated with the set of unobservable nodes, which need to be estimated using the model-X. Those $(2 \times n_{NOI})$ number of parameters that are needed to be estimated, are the parameters of the optimization. However, each of the n_{NOI} sets of active and reactive powers will need to have its own sets of equations consisting of $(2 \times n_{NOI})$ number of parameters. Thus the total number of parameters that need to be estimated using the optimization objective is $(2 \times n_{NOI})^2$. This is the minimum number of observations needed to maintain the number of equations to be equal to the number of unknowns in the inverse mapping component of model-X. Thus, maintaining this minimum number of observations provides a theoretical guarantee to obtain unique solutions for those unknown parameters by ensuring invertibility of the library function matrix.

2) Matrix Sizes for Model-X Components: The matrices $\boldsymbol{x}$ and $\boldsymbol{y}$ are time series data. The structure of the matrix $\boldsymbol{y}$ consisting of active and reactive power measurements is (Number of measurements $\times$ 2 $\times$ Dimension of the system). The 2 in the dimension of the system is to account for the components corresponding to both the active and reactive powers of the corresponding nodes of the system. The matrix $\boldsymbol{x}$ consisting of the real and imaginary components of the voltage phasor of a particular node is a time series data. The structure of the matrix is (Number of measurements $\times$ 2 $\times$ Dimension of the system). The 2 in the dimension of the system is to account for both the u and w, representing the rectangular coordinates of the voltage phasors of the corresponding nodes of the system.

G. GIS Information Usage

The prior information about the parameters associated with the observable nodes using GIS information aid the performance of the mapping functions. As described in Step 4 of Algorithm 1, the prior information about the parameters associated with the observable nodes using GIS information reduces the computational burden, thereby aiding the performance of the mapping functions. This is achieved by using the spatial data of location and topology corresponding to the observable nodes obtained from the GIS database. The goal is to narrow down the parameters for estimation. As a result, the parameters corresponding to the observable nodes are estimated using the regression-based parameter learning approach. Using the parameter values as constraints in the latent layer results in estimating the parameters associated with the neighboring buses to the unobservable nodes. This results in the reduction of the computational complexity of the optimization algorithm based on the amount of unobservability, independent of the dimension of the system. Therefore, the prior information about the parameters associated with the observable nodes by using GIS information reduces the computational burden. Using this prior information as a constraint in the complete optimization objective, parameters corresponding to the unobservable nodes are then estimated. Therefore, the prior information about the parameters associated with the observable nodes aids the performance of the mapping functions. The numerical result for the reduction in the computational burden due to GIS is presented in Section V-D.

IV. Performance Guarantees for Quantifying Uncertainties

Considering the structural architecture of the proposed model-X, we need to measure the uncertainty of the model to ensure confidence in the performance of the model. As latent space is typically used to generate new samples with similar properties, the latent node generated by the intermediate mapping is used to incorporate this uncertainty using the Bayesian perspective [40]. Hence, the uncertainty quantification is performed using a Bayesian architecture inspired by [41] and [42]. The proof for the confidence interval of the proposed method is introduced in the Theorem 1.

Theorem 1 (Confidence Interval for the Model-X): For $d \in \mathbb{N}$ representing the dimensionality of $\boldsymbol{y}_{\mathcal{O}}$, Σ^+ representing the pseudoinverse of $\mathbb{E}[\Sigma]$, and $\nu = \min\{N_{MC}, d\}$ degrees of freedom for the chi-squared distribution of the probability $\mathbb{P}$ for the $\chi^2(P)$ function, the confidence interval for the reconstructed $\boldsymbol{y}_{\mathcal{O}}^{(m)}$ $\forall\ m \in [1, d]$ is:

$$\left[\mathbb{E}\left[\boldsymbol{y}_{\mathcal{O}}^{(m)}\right] - \sqrt{\chi_\nu^2(P)}\left\|u_n^T S^{\frac{1}{2}}\right\|_2, \mathbb{E}\left[\boldsymbol{y}_{\mathcal{O}}^{(m)}\right] + \sqrt{\chi_\nu^2(P)}\left\|u_n^T S^{\frac{1}{2}}\right\|_2\right]$$

where u_m^T denotes the m^{th} row of the matrix U, where $\mathbb{E}[\Sigma] = USU^T$, by using singular value decomposition.

Proof: Based on [41], the posterior distribution for the decoder part of Model-X, $\mathbb{P}(\boldsymbol{y}_{\mathcal{O}} \mid \boldsymbol{x}_{\mathcal{O}})$ is predicted using the following.

$$\begin{aligned}\mathbb{P}(\boldsymbol{y}_{\mathcal{O}} \mid \boldsymbol{x}_{\mathcal{O}}) &= \lim_{N_{MC}\to\infty}\int \mathbb{P}\left(\boldsymbol{y}_{\mathcal{O}} \;\middle|\; \boldsymbol{x}_{\bar{\mathbb{O}}}, \boldsymbol{x}_{\mathcal{O}}\right)\mathbb{P}\left(\boldsymbol{x}_{\bar{\mathbb{O}}} \;\middle|\; \boldsymbol{x}_{\mathcal{O}}\right)d\boldsymbol{x}_{\bar{\mathbb{O}}}\\ &= \frac{1}{N_{MC}}\sum_{j=1}^{N_{MC}}\mathbb{P}\left(\boldsymbol{y}_{\mathcal{O}} \;\middle|\; \boldsymbol{x}_{\bar{\mathbb{O}}}^{(j)}, \boldsymbol{x}_{\mathcal{O}}\right). \end{aligned} \tag{7}$$

The sampling from latent space has been used to estimate the confidence region for prediction uncertainty of the trained model. Using the Monte-Carlo estimator, the mean prediction value $\mathbb{E}[\boldsymbol{y}_{\mathcal{O}}]$ and the empirical co-variance matrix $\mathbb{E}[\Sigma]$ can be obtained. The empirical standard deviation is $\hat{\sigma} = \sqrt{\mathrm{diag}(\mathbb{E}[\Sigma])}$. To estimate the confidence interval, let us assume $\mathbb{P}(\boldsymbol{y}_{\mathcal{O}}|\boldsymbol{x}_{\mathcal{O}}) \sim \mathcal{N}(\mu, \sigma)$, where $\mathbb{E}[\boldsymbol{y}_{\mathcal{O}}]$ and $\mathbb{E}[\Sigma]$ are approximations to μ and σ, as obtained above from N_{MC} samples. Hence, the confidence interval estimate for $\boldsymbol{y}_{\mathcal{O}}$ is given as follows:

$$\begin{aligned}\boldsymbol{y}_{\mathcal{O}}^{(i)} \in \mathbb{R}^d : &\left(\boldsymbol{y}_{\mathcal{O}}{}^{(j)} - \mathbb{E}\left[\boldsymbol{y}_{\mathcal{O}}{}^{(j)}\right]\right)\Sigma^+\left(\boldsymbol{y}_{\mathcal{O}}{}^{(j)} - \mathbb{E}\left[\boldsymbol{y}_{\mathcal{O}}{}^{(j)}\right]\right)^T\\ &\leq \chi_\nu^2(P),\end{aligned} \tag{8}$$

where $\chi^2(P)$ is the quantile function for probability $\mathbb{P}$ of the chi-squared distribution with $\nu = \min\{N_{MC}, d\}$ degrees of freedom. Here, $d \in \mathbb{N}$ represents the dimensionality of $\boldsymbol{y}_{\mathcal{O}}$, and Σ^+ represents the pseudoinverse of $\mathbb{E}[\Sigma]$. Now, using singular value decomposition, $\mathbb{E}[\Sigma] = USU^T$, where u_m^T denotes the m^{th} row of the matrix U. Hence, the interval for $\boldsymbol{y}_{\mathcal{O}}^{(m)}$ $\forall\ m \in [1, d]$ is:

$$\left[\mathbb{E}\left[\boldsymbol{y}_{\mathcal{O}}^{(m)}\right] - \sqrt{\chi_\nu^2(P)}\left\|u_n^T S^{\frac{1}{2}}\right\|_2, \mathbb{E}\left[\boldsymbol{y}_{\mathcal{O}}^{(m)}\right] + \sqrt{\chi_\nu^2(P)}\left\|u_n^T S^{\frac{1}{2}}\right\|_2\right]$$

■

The theorem provides the upper and lower bound on the estimation error for the reconstruction of the measurement values. The bounds are defined by the expected value of the reconstructed measurements with the deviation characterized by the quantile function for the probability of the chi-squared distribution and the empirical covariance matrix of the reconstructed power values using the latent variables, which can be obtained by using the Monte-Carlo estimator. The reconstruction is performed by considering the unobservability as latent units. Thus, by using additional information the knowledge about the partial state of the system is inferred, which bounds the uncertainty in the reconstruction of the measurement values. The numerical result for the uncertainty bound of the proposed method is presented in Section V-E.

V. Simulations

The contributions of this work are validated numerically for a diverse selection of power grid distribution test cases from MATPOWER [37]. For these MATPOWER test cases, the proposed method is trained to optimize the objective given in Equation (6).

A. Training Method for Model-X

To optimize the objective function, the backpropagation algorithm, as described in [43] and Levenberg-Marquardt optimization algorithm [44], are used as the training functions. With the training function as described above, the mean squared error function is used as the performance function to achieve optimization of the objective function. To improve the conditioning of the optimization problem, the data is preprocessed by normalizing the data to the interval $[-1,\ 1]$. The data is randomly divided into training, testing, and validation data sets. The first 70% of the data is assigned for training the model, 15% for the validation set to generalize the model, and the remaining 15% of the data is used for an independent testing of the model generalization. The training, validation, and testing data are obtained from the same observable nodes to maintain consistency of the mean squared error calculations for model training and generalization. The loss in the estimation of the system parameters is considered the performance metric for comparing the different scenarios. All scenarios are trained for a maximum solver iteration of 400 using a Precision 5820 Tower Workstation, implemented with $1e^{-6}$ being the lower bound on the change in the value of the objective function during a step.

For optimization of the objective function in Equation (6), the parameters of the network are initialized randomly. A neural network with a symbolic regression algorithm is implemented to form the combined forward and inverse mapping objective function. The number of neural network layers is considered as five throughout the experiment. For the analysis, the number of hidden nodes is determined based on a hyperparameter using a heuristic method, which is dependent on the number of observable nodes in the system. This accounts for the rectangular coordinate representation of the physical law-based power flow mapping as described in Equation (10) in the paper.

However, as the level of unobservability changes the model need not be changed. When the model is initialized with the number of hidden nodes depending on the number of observable nodes in the network, the hidden nodes learn the

TABLE I
COMPARISON OF PERFORMANCE FOR THE MODEL WITH AND WITHOUT USING BLENDING TECHNIQUE TO TACKLE CHANGES IN TOPOLOGY

Percentage Reconstruction Performance			
Description	Original Topology	Changed Topology	
		Without Blending	With Blending
Moderate Change	99.97%	91.85%	99.95%
Severe Change		87.38%	99.90%

representation associated with the observable nodes for the forward mapping function. However, as the observability changes moderately, the model does not need to change as the existing number of hidden nodes are still capable of learning the representation for the observable nodes associated with the new level of unobservability. The model tackles the changing observablility by using a sample-wise dynamic network method based on blending network parameters while maintaining a fixed model architecture [45]. The way this has been achieved is by considering the model parameters associated with the common topological nodes before the topology change and blending those parameters for training the model considering the new topological change. The result showing the performance in terms of reconstruction loss with and without using the parameter blending technique is shown in Table I. Therefore, upon using the parameter blending technique, when the level of unobservability changes, the forward mapping information obtained from the model using the original level of unobservability will be further enhanced by the new information obtained from the changing observability. This new information will be obtained from the changing representation learning by the hidden nodes in response to the changing observability. As a result, this makes the model more robust and helps in reinforcing the new information on the foundation of the earlier learning. In addition, the rectifier or ReLU activation function is used for training the neural network in the forward mapping part of model-X. ReLU activation function is defined as: $f(a) = a^+ = \max(0, a)$, where a is the input to a neuron. Levenberg-Marquardt training, as discussed in [46], is used to optimize the objective function in Equation (6).

With the training method described above, IEEE standard power system models are introduced for the experiment. The proposed method is relevant to the power systems domain primarily because of three premises. First, in the case of power systems, there exists a form of physics in terms of voltage and power mapping, which results in latent variables interacting with particular basis functions only. Second, the estimation of the unobservability as a function of known power measurements is possible because there exists an inherent knowledge about the unobservability. This knowledge about the unobservability is derived partially from the power measurements. Third, the introduction of the latent layer increases the learning capability of the model by learning the inverse mapping, thereby estimating the system parameters. A detailed description of the problem setup and the data preparation for a power system test case is described below.

B. Data Generation for Model Evaluation

With the training method described above, unobservability is randomly selected among the nodes of the system. It represents the components that creates partial system observability. In addition, one of the buses is selected as the slack (reference) bus, as one bus in the power system topology needs to be the slack bus; the phase angle values for all the observations corresponding to that particular bus are considered as zero radians. This is used for the initial calculation of the measurements. The set of equations representing the physical power flow mapping in a power system is represented in Equation (9).

$$p_i = \sum_{k=1}^{n} |v_i||v_k|(g_{ik}\cos\phi_{ik} + b_{ik}\sin\phi_{ik}),$$
$$q_i = \sum_{k=1}^{n} |v_i||v_k|(g_{ik}\sin\phi_{ik} - b_{ik}\cos\phi_{ik}), \tag{9}$$

where $i = 1, \ldots, n$, n being the number of buses in the system. p_i and q_i represents the total real and reactive power injections at bus i, g_{ik} and b_{ik} represent the conductance and the susceptance values corresponding to the $(i,k)^{th}$ element of the bus admittance matrix, δ_i is the phase angle for the i^{th} bus voltage, δ_k is the phase angle for the k^{th} bus voltage, and ϕ_{ik} is the difference of the phase angles for the i^{th} and k^{th} bus, defined as $\phi_{ik} = \delta_i - \delta_k$. To use the symbolic regression-based inverse mapping, the rectangular coordinates of the voltage phasors have been used to represent the power-flow mappings, as the rectangular coordinate representation simplifies the trigonometric functions to polynomial functions [15]. The physical law-based power flow mapping is represented in Equation (10).

$$p_i = \sum_{k=1}^{n}(u_i u_k g_{ik} + w_i w_k g_{ik} + w_i u_k b_{ik} - u_i w_k b_{ik}),$$
$$q_i = \sum_{k=1}^{n}(w_i u_k g_{ik} - u_i w_k g_{ik} - u_i u_k b_{ik} - w_i w_k b_{ik}), \tag{10}$$

where $u_i = |v_i|\cos\phi_i$, and $w_i = |v_i|\sin\phi_i$, denote the real and imaginary components of the voltage phasor of node i respectively.

To analyze the performance robustness of model-X against unobservability, multiple levels of unobservability are introduced into the test systems under consideration. For the different networks considered for simulating model-X, a variable number of unobservable nodes within a percentage of 10% to 50% has been selected. The consideration of the unobservability within a percentage of 10% to 50% is selected based on the input provided by our utility partners. The unobservable nodes in this case introduce the noise in the system. To analyze the impact of unobservability on the performance of model-X, we have compared the performance of model-X as the unobservability in the system increases. We have presented the result in Figure 4. The result is in terms of the normalized error magnitude for the estimation of system parameters,

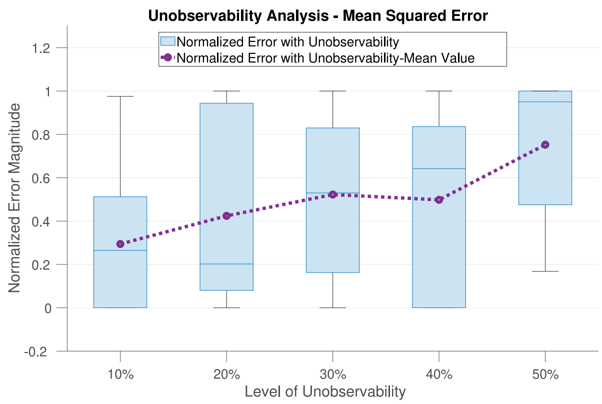

Fig. 4. Comparison of performance for multiple levels of unobservability in a partially observable system.

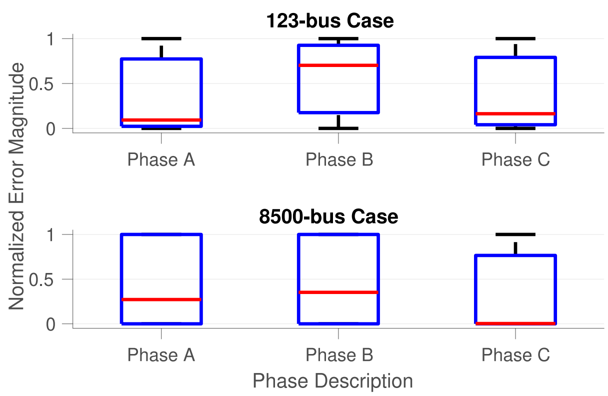

Fig. 5. Comparison of performance for the individual phases of multiphase system in a partially observable system.

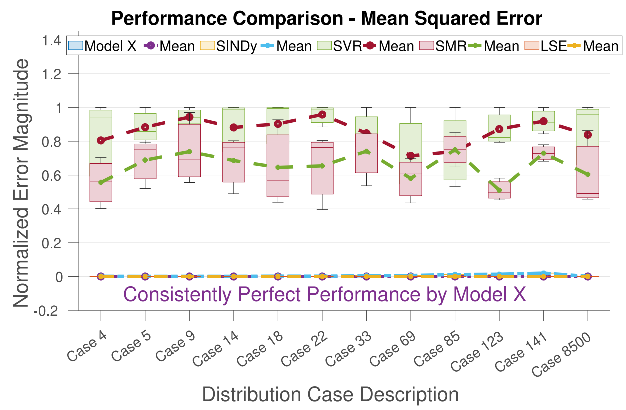

Fig. 6. Comparison of performance in a partially observable system. *Model-X: Proposed Method, SINDY based on [48], SVR based on [15], SMR based on [29], LSE based on [30].*

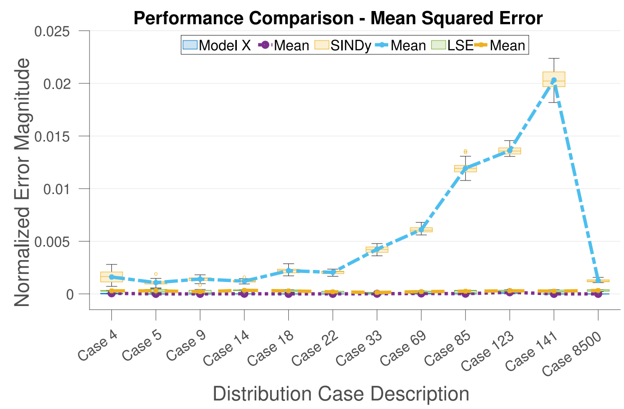

Fig. 7. Comparison of model-X performance against SINDy [48] and the method proposed in [30] in a partially observable system.

averaged over all the test cases. From the analysis, it can be observed that the analysis based on the level of unobservability is very important to the study of the performance of model-X, which suggests that the level of unobservability does not weaken the capability of model-X.

With the above problem setup, we introduce IEEE standard power system models in the high-level simulation toolbox MATPOWER [37] based on MATLAB. For the experiments, we considered IEEE 4-bus, 5-bus, 9-bus, 14-bus, 18-bus, 22-bus, 33-bus, 69-bus, 85-bus, 123-bus, 141-bus and 8500-bus test case systems. The 123-bus and 8500-bus multiphase unbalanced systems do not exist in MATPOWER. So we used the test cases from [47]. We extended the proposed method for the three-phase system by considering the complete system for simulation as well as performing the simulation on individual phases of the 3-phase system test case. The performance of model-X on the individual phases of the 123-bus test case has been visualized in Figure 5. The 3 phases behave in a similar manner as that of independent single phases, thereby, verifying the generalizability capability of model-X. Further, the scalability and applicability of the proposed method in real-life applications have been verified. This is achieved by verifying the performance of model-X using systems up to the IEEE 8500-node test case. Hence, these results verify the generalizability capability of model-X.

C. Forward and Inverse Mapping: Estimation of System Parameters

By using model-X, the estimation of parameters corresponding to the buses, which are not connected to the unobservable bus directly, is accurate, with no noise in the estimation. In addition, the parameters associated with the unobservable nodes are also estimated, which was otherwise impossible to find using simple regression or even an optimization involving inverse mapping only. Considering the strengths and the advantages of model-X, the comparison of different methods against model-X in estimating the system parameters is visualized in Figures 6, 7 and 8. From those figures, it can be observed that the model-X outperforms the methods proposed by [15], [29], or [30].

For the purpose of validation, we have used the SINDy algorithm [48] based on a compressive sensing based technique as discussed in [49], and the methods proposed in [15], [29], and [30], for comparing the performance of the proposed model-X. The analysis is performed on multiple power system cases with 25 runs each, and the mean and variance of the error values are shown in Figures 6, 7, 8. The performance comparison of model-X against the earlier methods is shown to validate the consistently perfect system parameter estimation capability of model-X, which proves the forward and inverse mapping capability of model-X.

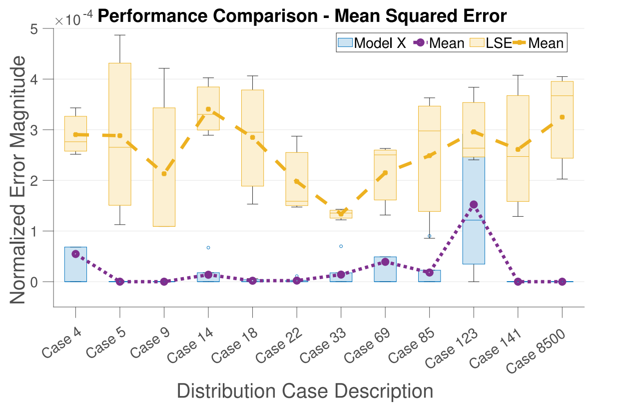

Fig. 8. Comparison of model-X performance against the method proposed in [30] in a partially observable system.

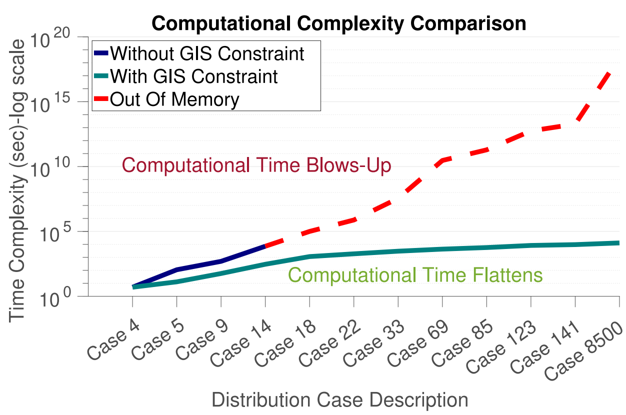

Fig. 9. Comparison of computational time.

D. Improvement in Computational Complexity

By using GIS data as a constraint for the optimization function in Equation (6), the required number of system states is reduced for estimating the unobservability. Obtaining an adequate number of system states using GIS results in reducing the number of library functions to estimate the system parameters using symbolic regression. This helps in reducing the complexity of optimization. Hence, by using GIS information, the computational complexity of the model is improved by embedding the network size into the latent layers. It leads to an improvement from exponential growth to linear growth in terms of the number of parameters, with an increase in the number of dimensions for the cases under consideration, as shown in Table II. The comparison of computational time for using GIS information is shown in Figure 9. This validates the significant improvement in the computational complexity of the model-X. In Figure 9, the OoM (Out-of-Memory) time points are determined by mapping the known computational time against the number of parameters to be optimized using non-linear regression.

E. Estimation Confidence of Model-X

The estimation of parameters corresponding to the nodes which are connected directly to the unobservable bus is obtained accurately by using the two-way information flow,

TABLE II
COMPARISON OF NUMBER OF PARAMETERS WITH AND WITHOUT USING GIS INFORMATION

Contribution 2: Number of Parameters			
Case Description	Forward Mapping	Intermediate Mapping	Inverse Mapping
Without GIS Constraint	$k_1 + k_2 \times n$	$k_3 \times n$	$n \times \binom{n}{2}$
With GIS Constraint	$k_1 + k_2 \times n$	$k_3 \times n$	$k_4 \times n$

*Note: k_1, k_2, k_3, and k_4 represent the constant of proportionality.

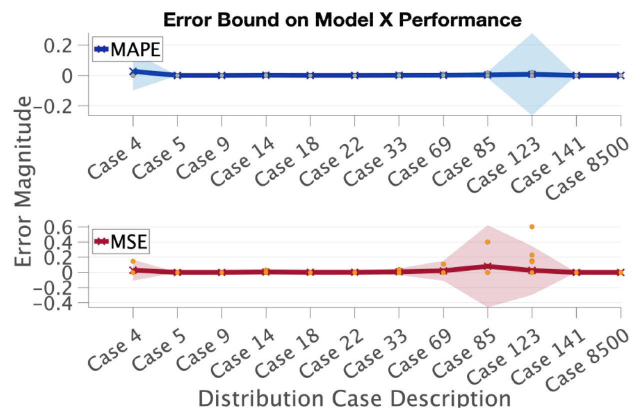

Fig. 10. Confidence of Model-X in two-way information flow in presence of an unobservable component.

which otherwise would not be possible using the existing methods. The confidence interval (CI) for the performance of model-X in terms of the two-way information flow is shown in Figure 10. It is important to note here that, the y-axis scale while obtaining the confidence interval is determined by data points in terms of estimation error for the posterior distribution. So, the plot revolves around the zero value because the mean value of the error revolves around zero. However, as certain points in terms of the posterior estimation error also falls beyond the zero mean value due to the variable standard deviation, this is captured by the confidence interval region as shown in the Figure 10. Hence, to improve the clarity of the posterior estimation error with different distribution networks, an improved figure based on a logarithmic scale for the y-axis has also been plotted, which is shown in Figure 11. This captures the mean value of the posterior estimation error with improved clarity.

VI. CONCLUSION

We present a solution to the problem of providing robust monitoring capability for secondary distribution systems in data-limited scenarios by inferring system physics information. It has played a key role in a variety of research directions. These include controllability of the energy grid, state estimation, attack detection in a power grid, enhancing the functionality, and performance of the grid edge system, etc. This work shows that it is possible to achieve superior mapping capability to learn the underlying physical information of the systems, even with limited observability using consistent

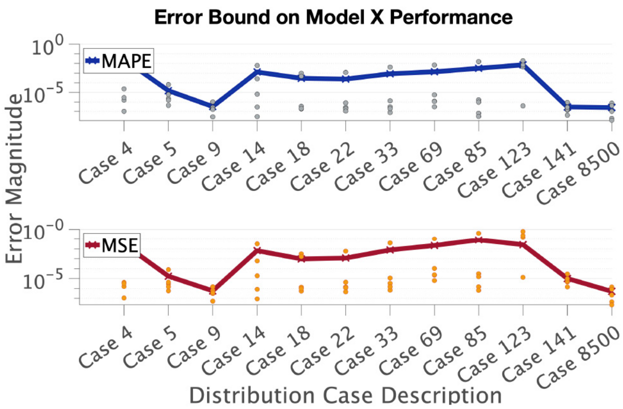

Fig. 11. Logarithmic Confidence of Model-X in two-way information flow in presence of an unobservable component.

two-way mapping and the latent layer design with network size and latent units. The proposed method shows strong performance on the benchmarks in the power domain. In addition to the improved mapping performance, the method focus on understanding the relationship of latent units to measurements. Based on the numerical results, the proposed method is capable of estimating the system parameters with high accuracy in presence of partial observability of the system. It involves all system components, including those interacting directly with the unobservability. Moreover, the improvement in the computational complexity achieved by embedding the network size into the latent layers applies to a wide range of results using GIS information. It suggests that the proposed model can adapt to any dimension of power system cases. Improvement of the mapping and computational capability ensures a robust and accurate model for a sustainable and reliable energy system operation. This model provides confidence in the mapping. Thus, the model has the potential to form the next generation of power grid management systems with design consistency, maximized physical explainability, and confidence. This will instill trust in the AI for distribution system edges with unobservability.

REFERENCES

[1] L. Nutter and J. Baumann. "Distributed energy resources technical considerations for the bulk power system." Federal Register, Nation Archive. Apr. 2018. [Online]. Available: https://www.federalregister.gov/documents/2018/05/04/2018-09450/distributed-energy-resources-technical-considerations-for-the-bulk-power-system-notice-inviting

[2] "Growth opportunities in distributed energy, forecast to 2030." Frost and Sullivan. May 2020. [Online]. Available: https://www.reportlinker.com/p05894509/Growth-Opportunities-in-Distributed-Energy-Forecast-to.html

[3] S. Nalley and A. LaRose. "Annual energy outlook 2022." U.S. Energy Information Administration. Mar. 2022. [Online]. Available: https://www.eia.gov/outlooks/aeo/

[4] Y. Zhang, X. Wang, J. Wang, and Y. Zhang, "Deep reinforcement learning based volt-VAR optimization in smart distribution systems," *IEEE Trans. Smart Grid*, vol. 12, no. 1, pp. 361–371, Jan. 2021. [Online]. Available: https://doi.org/10.11%2Ftsg.2020.3010130

[5] J. Zhao *et al.*, "Power system dynamic state estimation: Motivations, definitions, methodologies, and future work," *IEEE Trans. Power Syst.*, vol. 34, no. 4, pp. 3188–3198, Jul. 2019. [Online]. Available: https://doi.org/10.11%2Ftpwrs.2019.2894769

[6] National Infrastructure Advisory Council. "Surviving a catastrophic power outage." Cybersecurity Infrastructure Security Agency. Dec. 2018. [Online]. Available: https://www.cisa.gov/publication/niac-catastrophic-power-outage-study

[7] S. Lefebvre, J. Prévost, and L. Lenoir, "Distribution state estimation: A necessary requirement for the smart grid," in *Proc. IEEE PES General Meeting Conf. Exposit.*, Jul. 2014, pp. 1–5. [Online]. Available: https://doi.org/10.11%2Fpesgm.2014.6939030

[8] C. N. Lu, J. H. Teng, and W.-H. E. Liu, "Distribution system state estimation," *IEEE Trans. Power Syst.*, vol. 10, no. 1, pp. 229–240, Feb. 1995. [Online]. Available: https://doi.org/10.11%2F59.373946

[9] M. E. Baran, "Challenges in state estimation on distribution systems," in *Proc. IEEE Power Eng. Soc. Transm. Distrib. Conf.*, Aug. 2001, pp. 429–433. [Online]. Available: https://doi.org/10.11%2Fpess.2001.970062

[10] S. Bhela, V. Kekatos, and S. Veeramachaneni, "Enhancing observability in distribution grids using smart meter data," *IEEE Trans. Smart Grid*, vol. 9, no. 6, pp. 5953–5961, Nov. 2018. [Online]. Available: https://doi.org/10.11%2Ftsg.2017.2699939

[11] A. S. Zamzam, X. Fu, and N. D. Sidiropoulos, "Data-driven learning-based optimization for distribution system state estimation," *IEEE Trans. Power Syst.*, vol. 34, no. 6, pp. 4796–4805, Nov. 2019. [Online]. Available: https://doi.org/10.11%2Ftpwrs.2019.2909150

[12] G. Wang, G. B. Giannakis, J. Chen, and J. Sun, "Distribution system state estimation: An overview of recent developments," *Front. Inf. Technol. Electron. Eng.*, vol. 20, no. 1, pp. 4–17, Jan. 2019. [Online]. Available: https://doi.org/10.16%2Ffitee.1800590

[13] C. Muscas, M. Pau, P. A. Pegoraro, and S. Sulis, "Effects of measurements and pseudomeasurements correlation in distribution system state estimation," *IEEE Trans. Instrum. Meas.*, vol. 63, no. 12, pp. 2813–2823, Dec. 2014. [Online]. Available: https://doi.org/10.11%2Ftim.2014.2318391

[14] K. A. Clements, "The impact of pseudo-measurements on state estimator accuracy," in *Proc. IEEE Power Energy Soc. General Meeting*, Jul. 2011, pp. 1–4. [Online]. Available: https://doi.org/10.11%2Fpes.2011.6039370

[15] J. Yu, Y. Weng, and R. Rajagopal, "Robust mapping rule estimation for power flow analysis in distribution grids," in *Proc. IEEE North Amer. Power Symp.*, Sep. 2017, pp. 1–6. [Online]. Available: https://doi.org/10.11%2Fnaps.2017.8107397

[16] D. D. Giustina, M. Pau, P. A. Pegoraro, F. Ponci, and S. Sulis, "Electrical distribution system state estimation: Measurement issues and challenges," *IEEE Instrum. Meas. Mag.*, vol. 17, no. 6, pp. 36–42, Dec. 2014. [Online]. Available: https://doi.org/10.11%2Fmim.2014.6968929

[17] L. Zhang, G. Wang, and G. B. Giannakis, "Going beyond linear dependencies to unveil connectivity of meshed grids," in *Proc. IEEE 7th Int. Workshop Comput. Adv. Multi-Sens. Adapt. Process. (CAMSAP)*, Dec. 2017, pp. 1–5. [Online]. Available: https://doi.org/10.11%2Fcamsap.2017.8313078

[18] J. Sexauer, P. Javanbakht, and S. Mohagheghi, "Phasor measurement units for the distribution grid: Necessity and benefits," in *Proc. IEEE PES Innov. Smart Grid Technol. Conf. (ISGT)*, Feb. 2013, pp. 1–6. [Online]. Available: https://doi.org/10.11%2Fisgt.2013.6497828

[19] H. H. Muller, M. J. Rider, C. A. Castro, and V. L. Paucar, "Power flow model based on artificial neural networks," in *Proc. IEEE Russia Power Tech*, Jun. 2005, pp. 1–6. [Online]. Available: https://doi.org/10.11%2Fptc.2005.4524546

[20] D. Singh, J. P. Pandey, and D. S. Chauhan, "Topology identification, bad data processing, and state estimation using fuzzy pattern matching," *IEEE Trans. Power Syst.*, vol. 20, no. 3, pp. 1570–1579, Aug. 2005. [Online]. Available: https://doi.org/10.11%2Ftpwrs.2005.852086

[21] R. Singh, E. Manitsas, B. C. Pal, and G. Strbac, "A recursive Bayesian approach for identification of network configuration changes in distribution system state estimation," *IEEE Trans. Power Syst.*, vol. 25, no. 3, pp. 1329–1336, Aug. 2010. [Online]. Available: https://doi.org/10.11%2Ftpwrs.2010.2040294

[22] W. Luan, J. Peng, M. Maras, J. Lo, and B. Harapnuk, "Smart meter data analytics for distribution network connectivity verification," *IEEE Trans. Smart Grid*, vol. 6, no. 4, pp. 1964–1971, Jul. 2015. [Online]. Available: https://doi.org/10.11%2Ftsg.2015.2421304

[23] B. Hayes, A. Escalera, and M. Prodanovic, "Event-triggered topology identification for state estimation in active distribution networks," in *Proc. IEEE PES Innov. Smart Grid Technol. Conf. Eur. (ISGT-Europe)*, Oct. 2016, pp. 1–6. [Online]. Available: https://doi.org/10.11%2Fisgteurope.2016.7856295

[24] G. Cavraro and R. Arghandeh, "Power distribution network topology detection with time-series signature verification method," *IEEE Trans. Power Syst.*, vol. 33, no. 4, pp. 3500–3509, Jul. 2018. [Online]. Available: https://doi.org/10.11%2Ftpwrs.2017.2779129

[25] G. Cavraro, V. Kekatos, and S. Veeramachaneni, "Voltage analytics for power distribution network topology verification," *IEEE Trans. Smart Grid*, vol. 10, no. 1, pp. 1058–1067, Jan. 2019. [Online]. Available: https://doi.org/10.11%2Ftsg.2017.2758600

[26] J. Zhang, Y. Wang, Y. Weng, and N. Zhang, "Topology identification and line parameter estimation for non-PMU distribution network: A numerical method," *IEEE Trans. Smart Grid*, vol. 11, no. 5, pp. 4440–4453, Sep. 2020. [Online]. Available: https://doi.org/10.11%2Ftsg.2020.2979368

[27] S. Powell, A. Ivanova, and D. Chassin, "Fast solutions in power system simulation through coupling with data-driven power flow models for voltage estimation," Jan. 2020, *arXiv:2001.01714*.

[28] K. P. Guddanti, Y. Weng, and B. Zhang, "A matrix-inversion-free fixed-point method for distributed power flow analysis," *IEEE Trans. Power Syst.*, vol. 37, no. 1, pp. 653–665, Jan. 2022. [Online]. Available: https://doi.org/10.11%2Ftpwrs.2021.3098479

[29] J. Yuan and Y. Weng, "Support matrix regression for learning power flow in distribution grid with unobservability," *IEEE Trans. Power Syst.*, vol. 37, no. 2, pp. 1151–1161, Mar. 2022. [Online]. Available: https://doi.org/10.11%2Ftpwrs.2021.3107551

[30] H. Li, Y. Weng, Y. Liao, B. Keel, and K. E. Brown, "Distribution grid impedance & topology estimation with limited or no micro-PMUs," *Int. J. Elect. Power Energy Syst.*, vol. 129, Jul. 2021, Art. no. 106794. [Online]. Available: https://doi.org/10.10%2Fj.ijepes.2021.106794

[31] V. Miranda, J. Krstulovic, H. Keko, C. Moreira, and J. Pereira, "Reconstructing missing data in state estimation with autoencoders," *IEEE Trans. Power Syst.*, vol. 27, no. 2, pp. 604–611, May 2012. [Online]. Available: https://doi.org/10.11%2Ftpwrs.2011.2174810

[32] P. N. P. Barbeiro, J. Krstulovic, H. Teixeira, J. Pereira, F. J. Soares, and J. P. Iria, "State estimation in distribution smart grids using autoencoders," in *Proc. IEEE Int. Power Eng. Optim. Conf.*, Mar. 2014, pp. 358–363. [Online]. Available: https://doi.org/10.11%2Fpeoco.2014.6814454

[33] Y. Lin and A. Abur, "Robust state estimation against measurement and network parameter errors," *IEEE Trans. Power Syst.*, vol. 33, no. 5, pp. 4751–4759, Sep. 2018. [Online]. Available: https://doi.org/10.11%2Ftpwrs.2018.2794331

[34] Y. Lin, J. Wang, and M. Cui, "Reconstruction of power system measurements based on enhanced denoising autoencoder," in *Proc. IEEE Power Energy Soc. General Meeting*, Aug. 2019, pp. 1–5. [Online]. Available: https://doi.org/10.11%2Fpesgm40551.2019.8973925

[35] Y. Lin and J. Wang, "Probabilistic deep autoencoder for power system measurement outlier detection and reconstruction," *IEEE Trans. Smart Grid*, vol. 11, no. 2, pp. 1796–1798, Mar. 2020. [Online]. Available: https://doi.org/10.11%2Ftsg.2019.2937043

[36] F. Coelho, M. Costa, M. Verleysen, and A. P. Braga, "LASSO multi-objective learning algorithm for feature selection," *Soft Comput.*, vol. 24, no. 17, pp. 13209–13217, Feb. 2020. [Online]. Available: https://doi.org/10.10%2Fs00500-020-04734-w

[37] R. D. Zimmerman, C. E. Murillo-Sánchez, and R. J. Thomas, "MATPOWER: Steady-state operations, planning, and analysis tools for power systems research and education," *IEEE Trans. Power Syst.*, vol. 26, no. 1, pp. 12–19, Feb. 2011. [Online]. Available: https://doi.org/10.11%2Ftpwrs.2010.2051168

[38] A. Monticelli, "Electric power system state estimation," *Proc. IEEE*, vol. 88, no. 2, pp. 262–282, Feb. 2000. [Online]. Available: https://doi.org/10.11%2F5.824004

[39] S. Bolognani, N. Bof, D. Michelotti, R. Muraro, and L. Schenato, "Identification of power distribution network topology via voltage correlation analysis," in *Proc. 52nd IEEE Conf. Decis. Control*, Dec. 2013, pp. 1659–1664. [Online]. Available: https://doi.org/10.11%2Fcdc.2013.6760120

[40] H. M. D. Kabir, A. Khosravi, M. A. Hosen, and S. Nahavandi, "Neural network-based uncertainty quantification: A survey of methodologies and applications," *IEEE Access*, vol. 6, pp. 36218–36234, 2018. [Online]. Available: https://doi.org/10.11%2Faccess.2018.2836917

[41] D. P. Kingma and M. Welling, "Auto-encoding variational bayes," in *Proc. Int. Conf. Learn. Represent.*, May 2014, pp. 1–14. [Online]. Available: http://arxiv.org/abs/1312.6114

[42] K. Gundersen, A. Oleynik, N. Blaser, and G. Alendal, "Semi-conditional variational auto-encoder for flow reconstruction and uncertainty quantification from limited observations," *Phys. Fluids*, vol. 33, no. 1, Jan. 2021, Art. no. 17119. [Online]. Available: https://doi.org/10.10%2F5.0025779

[43] Y. LeCun *et al.*, "Backpropagation applied to handwritten zip code recognition," *Neural Comput.*, vol. 1, no. 4, pp. 541–551, Dec. 1989. [Online]. Available: https://doi.org/10.11%2Fneco.1989.1.4.541

[44] R. H. Barham and W. Drane, "An algorithm for least squares estimation of nonlinear parameters when some of the parameters are linear," *Technometrics*, vol. 14, no. 3, pp. 757–766, Aug. 1972. [Online]. Available: https://doi.org/10.10%2F00401706.1972.10488964

[45] Y. Han, G. Huang, S. Song, L. Yang, H. Wang, and Y. Wang, "Dynamic neural networks: A survey," *IEEE Trans. Pattern Anal. Mach. Intell.*, early access, Oct. 6, 2021. [Online]. Available: https://ieeexplore.ieee.org/abstract/document/9560049

[46] F. D. Foresee and M. T. Hagan, "Gauss–Newton approximation to Bayesian learning," in *Proc. IEEE Int. Conf. Neural Netw.*, Aug. 2002, pp. 1930–1935. [Online]. Available: https://doi.org/10.11%2Ficnn.1997.614194

[47] K. P. Schneider *et al.*, "Analytic considerations and design basis for the IEEE distribution test feeders," *IEEE Trans. Power Syst.*, vol. 33, no. 3, pp. 3181–3188, May 2018. [Online]. Available: https://doi.org/10.11%2Ftpwrs.2017.2760011

[48] S. L. Brunton, J. L. Proctor, and J. N. Kutz, "Discovering governing equations from data by sparse identification of nonlinear dynamical systems," *Proc. Nat. Acad. Sci.*, vol. 113, no. 15, pp. 3932–3937, Mar. 2016. [Online]. Available: https://doi.org/10.10%2Fpnas.1517384113

[49] W.-X. Wang, R. Yang, Y.-C. Lai, V. Kovanis, and C. Grebogi, "Predicting catastrophes in nonlinear dynamical systems by compressive sensing," *Phys. Rev. Lett.*, vol. 106, no. 15, Apr. 2011, Art. no. 154101. [Online]. Available: https://doi.org/10.11%2Fphysrevlett.106.154101

Priyabrata Sundaray (Graduate Student Member, IEEE) received the B.Tech. degree in electrical and electronics engineering from SRM University, Kattankulathur, India, in 2014, and the M.S. degree in electrical engineering from the University of Wisconsin-Madison, USA, in 2019. He is currently pursuing the Ph.D. degree in electrical engineering with Arizona State University, Tempe, AZ, USA, where he is also serving as a Research Associate. In recognition of his extraordinary achievements, he received University Graduate Fellowship in 2020. His research interest focuses on the areas of interdisciplinary study of energy systems, and machine learning. The objective is to perform investigation of smart grids and determine relationship between the systems and the physics involved.

Yang Weng (Senior Member, IEEE) received the B.E. degree in electrical engineering from the Huazhong University of Science and Technology, Wuhan, China, the M.Sc. degree in statistics from the University of Illinois at Chicago, Chicago, IL, USA, and the M.Sc. degree in machine learning of computer science and the M.E. and Ph.D. degrees in electrical and computer engineering from Carnegie Mellon University, Pittsburgh, PA, USA. He joined Stanford University, Stanford, CA, USA, as the TomKat Fellow for sustainable energy. He is currently an Assistant Professor of electrical, computer, and energy engineering with Arizona State University, Tempe, AZ, USA. He received the CMU Dean's Graduate Fellowship in 2010, the Best Paper Award at the International Conference on Smart Grid Communication (SGC) in 2012, the First Ranking Paper of SGC in 2013, the Best Papers at the Power and Energy Society General Meeting in 2014, the ABB Fellowship in 2014, the Golden Best Paper Award at the International Conference on Probabilistic Methods Applied to Power Systems in 2016, and the Best Paper Award at IEEE Conference on Energy Internet and Energy System Integration in 2017, IEEE North American Power Symposium in 2019, and the IEEE Sustainable Power and Energy Conference in 2019.